LANGMUIR

pubs.acs.org/Langmuir Article

Chiral Sum Frequency Generation Spectroscopy Detects Double-Helix DNA at Interfaces

Ethan A. Perets, Kristian B. Olesen, and Elsa C. Y. Yan*

Cite This: https://doi.org/10.1021/acs.langmuir.2c00365 Read Online

ACCESS | Metrics & More | Article Recommendations | Supporting Information

ABSTRACT: Many DNA-based technologies involve the immobilization of DNA and therefore require a fundamental understanding of the DNA structure−function relationship at interfaces. We present three immobilization methods compatible with chiral sum frequency generation (SFG) spectroscopy at interfaces. They are the "anchor" method for covalently attaching DNA on a glass surface, the "island" method for dropcasting DNA on solid substrates, and the "buoy" method using a hydrocarbon moiety for localizing DNA at the air−water interface. Although SFG was previously used to probe DNA, the chiral and achiral SFG responses of single-stranded and double-stranded DNA have not been compared systemically. Using the three immobilization methods, we obtain the achiral and chiral C−H stretching spectra. The results introduce four potential applications of chiral SFG. First, chiral SFG gives null response from single-stranded DNA but prominent signals from double-stranded DNA, providing a simple binary readout for label-free detection of DNA hybridization. Second, with heterodyne detection, chiral SFG gives an opposite-signed spectral response useful for distinguishing native (D-) right-handed double helix from non-native (L-) left-handed double helix. Third, chiral SFG captures the aromatic C−H stretching modes of nucleobases that emerge upon hybridization, revealing the power of chiral SFG to probe highly localized molecular structures within DNA. Finally, chiral SFG is sensitive to macroscopic chirality but not local chiral centers and thus can detect not only canonical antiparallel double helix but also other DNA secondary structures, such as a poly-adenine parallel double helix. Our work benchmarks the SFG responses of DNA immobilized by the three distinct methods, building a basis for new chiral SFG applications to solve fundamental and biotechnological problems.

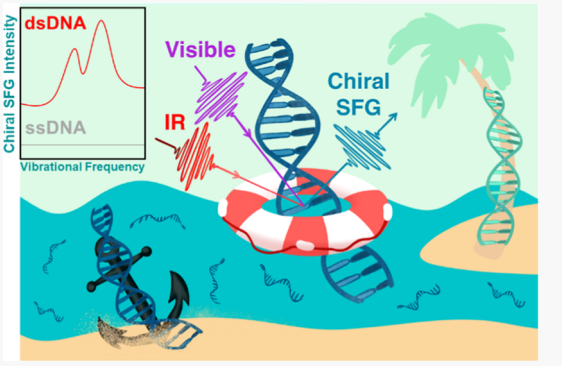

INTRODUCTION

Watson and Crick's discovery of the right-handed B-DNA double helix forever changed scientific understanding of DNA structure.[1] DNA was later shown to access a diversity of structures,[2,3] including left-handed Z-DNA,[4] G-quadruplexes,[5,6] and i-motifs.[7] Such DNA secondary structures have been implicated in genetic regulation[8,9] and cancer.[10,11] What are the chemical determinants of DNA structure? How does DNA structure regulate genomic activity? Answering these questions requires the development of analytical tools with high sensitivity to DNA structural diversity.

Over the last decade, chiral sum frequency generation (SFG) spectroscopy has emerged as a vibrational method that is sensitive to the macroscopic chirality of macromolecular and supramolecular structures at interfaces.[12−18] Chiral SFG can distinguish secondary structures of proteins[12,13,19,20] and other biomolecules.[21,22] Unlike X-ray crystallography[23−30] or NMR,[31−36] chiral SFG is real-time and *in situ*. Chiral SFG can probe a wide variety of physical states, including aqueous solutions and gels, under various experimental conditions, such as temperature, pH, and ionic strength. Chiral SFG probes the vibrational structures of molecules and therefore does not require molecular labels. Its chiral optical response predominantly arises from the electric dipole and polarizability of chiral molecules and does not rely on the relatively weak response from magnetic dipole like vibrational circular dichroism[37−42] or electric quadrupole like Raman optical activity.[43−46] Hence, relative to these linear chiral optical methods, chiral SFG can achieve high sensitivity. Chiral SFG also utilizes ultrafast lasers for time-resolved studies of the structural dynamics of biomacromolecules,[47] potentially applicable to probe ultrafast dynamics of solvation[48] and vibrational energy-transfer relaxation pathways.[49] Furthermore, under the dipole approximation, chiral SFG is allowed from chiral interfaces with macroscopic uniaxial (C_∞) symmetry but suppressed from isotropic bulk and thus is interface specific.[50] These advantages make chiral SFG an attractive method for probing the macroscopic chiral secondary structures of DNA at

Received: February 12, 2022
Revised: April 13, 2022

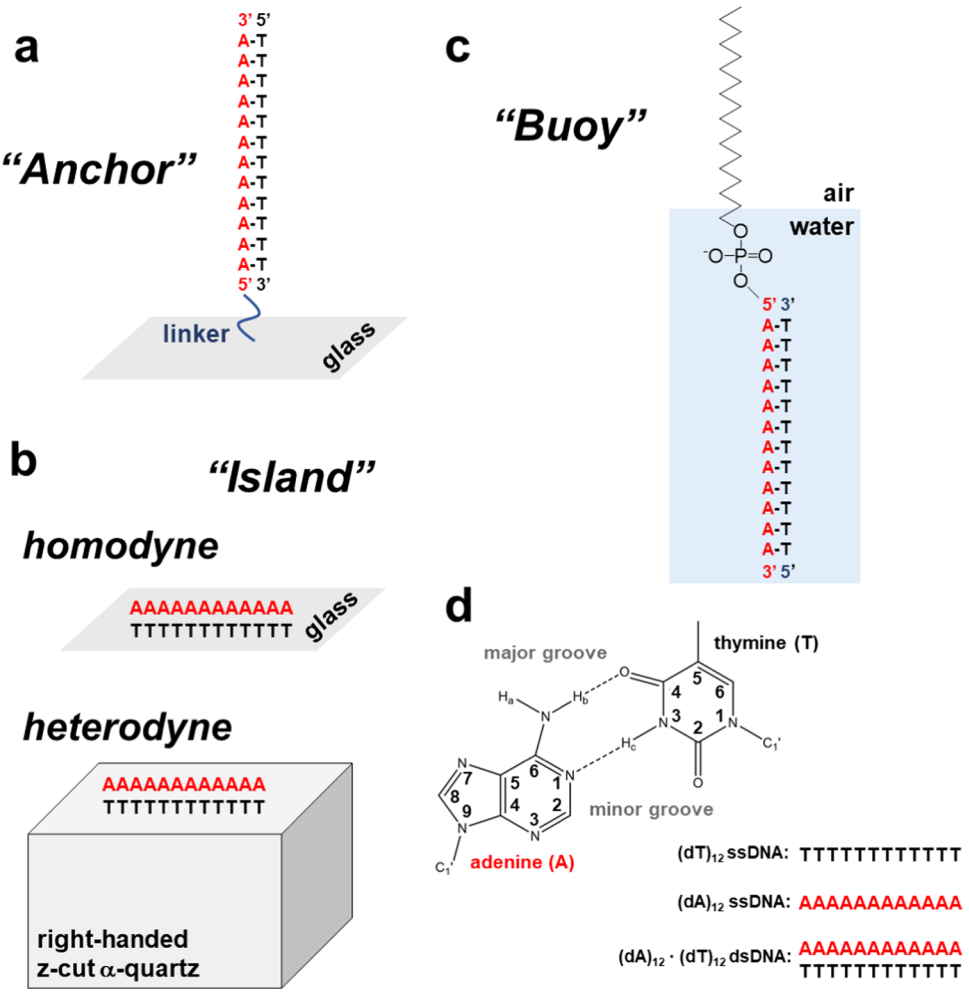

Figure 1. Methodologies for preparing DNA samples for SFG studies. (a) Anchor method: immobilization of DNA at the air−glass interface using covalent linkage. (b) Island method: immobilization of DNA at the air−glass or crystalline quartz interface by dropcasting. (c) Buoy method: immobilization of DNA at the air−water interface using a 5′ stearyl (C_{18}) hydrocarbon moiety. (d) Molecular structure of an adenine−thymine base pair and the ssDNA and dsDNA oligomers used in this study.

interfaces, with the potential for combining with vibrational microscopies[51] and other imaging technologies[52] for *in vitro* and live cell studies.

To realize these advantages, the robustness of the SFG response must first be benchmarked against a variety of interfacial preparatory platforms for a well-defined DNA secondary structure. The same DNA sequence and structure are not guaranteed to give the same SFG response when prepared at different interfaces or even at the same interface but under different methods for immobilizing DNA at the interface.[53,54] This is because SFG response is sensitive not only to the structures of biomacromolecules but also to the orientations of molecules at interfaces.[55−63]

In this report, we examine the achiral and chiral SFG responses of double-stranded DNA (dsDNA) and single-stranded DNA (ssDNA) using various immobilization methodologies at the air−glass, air−quartz, and air−water interfaces (Figure 1). Understanding DNA chemical behaviors at air interfaces is critical to the development of materials science applications and biotechnologies. DNA positioning at air−solid interfaces is useful for nanofabrication of DNA-based nanostructures on solid substrates,[64,65] quantitative physical mapping of genes,[66−68] and transmission electron microscopy DNA sequencing.[69] Despite being a strongly polar, hydrophilic biomacromolecule, DNA significantly adsorbs at the hydrophobic air−water interface in millimolar salt buffer[70] or upon DNA condensation from picomolar DNA concentrations in a bulk aqueous solution.[71] Accumulation of DNA at the air−water interface can enable various chemical processes relevant to the prebiotic origins of cellular life. For instance, the presence of a temperature gradient of 20 °C across the air−water interface was shown to concentrate DNA at the interface and to encourage encapsulation of DNA in vesicles, two conditions necessary to the emergence of biological cells.[72]

We study model systems of $(dA)_{12}\cdot(dT)_{12}$ dsDNA and its constituent $(dA)_{12}$ and $(dT)_{12}$ ssDNA (Figure 1). In general, poly(dA)·poly(dT) sequences have been characterized extensively by spectroscopic and structural methods, including infrared,[73−79] Raman,[80,81] circular dichroism,[82−86] X-ray crystallography,[23,25−28,87] NMR,[31] and several prior SFG studies (see also the Results and Discussion section).[88−90] Hybridized poly(dA)·poly(dT) sequences adopt the α-H-DNA (also called B′) double-helix structure.[25] The B′ structure is similar to canonical B-DNA but features a narrower minor groove and a periodic helical turn of 10 base pairs compared to 10.5 for B-DNA.[87] Moreover, the poly(dA)·poly(dT) duplex is relatively insensitive to hydration content, as it does not undergo the usual B-DNA to A-DNA transition upon

https://doi.org/10.1021/acs.langmuir.2c00365
Langmuir XXXX, XXX, XXX−XXX

dehydration.[91,92] These unique structural and dynamical characteristics allow poly(dA)·poly(dT) dsDNA to function *in vivo*, where these sequences are prevalent in promoter regions in yeast.[26,93]

Here, we compare achiral and chiral SFG vibrational responses of DNA oligomers in the C−H stretching region when DNA is covalently attached at the air−glass interface (the "anchor" method, Figure 1a), dropcast at the air−glass and the air−quartz interfaces (the "island" method, Figure 1b), and localized at the air−water interface using a hydrocarbon moiety (the "buoy" method, Figure 1c). In all cases, we observe achiral SFG response for both ssDNA and dsDNA. In contrast, chiral SFG is muted to unhybridized ssDNA but provides prominent signals for hybridized dsDNA. These results support that the three sample preparatory platforms can be combined with chiral SFG to provide straightforward, background-free, and label-free readouts to detect DNA double helices. When using the buoy method, we do not observe any chiral SFG signals from $(dT)_{12}$ ssDNA. However, we unexpectedly observe chiral signals from $(dA)_{12}$ ssDNA. We attribute this signal to a parallel double-helix structure formed by two molecules of $(dA)_{12}$ ssDNA. This noncanonical base pairing with homo-adenine base pairs was first reported for RNA by Watson and Crick[94,95] and was later observed for DNA oligomers.[96−103] The result indicates the promise of chiral SFG in detecting DNA secondary structures besides the quintessential antiparallel double helix. We also use heterodyne detection and observe native (D-) right-handed double helix, and non-native (L-) left-handed double helix give chiral SFG response in opposite signs, revealing the application of distinguishing enantiomeric DNA structures. The heterodyne spectra also resolve aromatic C−H stretching bands from nucleobases, revealing the capacity of chiral SFG in probing highly specific chemical structures within double-helix structures. Altogether, our study provides the groundwork for applying the anchor, island, and buoy interfacial preparatory platforms in developing SFG methods for sensing DNA hybridization and characterizing DNA structures at interfaces for diverse scientific and technological applications.

EXPERIMENTAL SECTION

Covalent Attachment of DNA Oligomers on Glass. Glass slides (Thermo Scientific, Cat. No. 420-004T, 101616-3) were cleaned in a plastic slide holder with 1:1 (v/v) HPLC-grade methanol and hydrochloric acid and then rinsed with deionized water and dried under nitrogen. The glass slides were then submerged in 30 mL of methanol containing 1.2 mL of (3-aminopropyl)triethoxysilane (APTES, 99%, Aldrich, Cat. No. 440140). The slide holder with the solution and glass slides was inverted to mix. The solution with glass slides was sonicated in the slide holder in cycles of 15 min ON, followed by 15 min OFF, for a total ON time of 2 h. Following sonication, the glass slides were washed in the slide holder five times, with 30 mL of HPLC-grade methanol each time, and then dried under nitrogen.

The APTES-functionalized glass slides were then transferred to custom slide holders made of glass (Scientific Glassblowing Laboratory, Yale University, New Haven, CT). Distilled, dry dimethylformamide containing 0.3% triethylamine (≥99%, Aldrich, Cat. No. T0886) was combined with HATU (97%, Aldrich, Cat. No. 445460) to a final concentration of HATU of 10 mM and mixed well, whereupon the solution became a deep yellow. The *para*-4-azidobenzoic acid (0.2 M in *tert*-butyl methyl ether, ≥95%, Aldrich, Cat. No. 778877) was then added to a final concentration of 5.5 mM, and the solution was directly transferred to the slide holder. With shaking, the reaction proceeded overnight. The azide-functionalized glass slides were then washed three times with methanol, followed by washing three times with deionized water, and then dried under nitrogen.

Finally, ssDNA or dsDNA was immobilized on the glass slides. The $(dA)_{12}$ ssDNA was synthesized (Oligo Synthesis Resource, Yale University) with a 5′ DBCO-TEG functionality (Glen Research, Sterling, VA, Cat. No. 10-1941). To prepare dsDNA, the 5′ DBCO-TEG-functionalized $(dA)_{12}$ ssDNA (180 μM in ddH_2O) was mixed in equal volume with the complimentary $(dT)_{12}$ ssDNA (200 μM in ddH_2O), lacking the 5′ functionality. The solution was heated in a water bath to 80 °C for 10 min and cooled slowly at room temperature. For ssDNA, the 5′-functionalized $(dA)_{12}$ was diluted in ddH_2O to a final concentration of 90 μM and subjected to the same heating/cooling process. Either dsDNA or ssDNA was adsorbed (100 μL) to one face of the azide-functionalized glass slide. The reaction proceeded overnight. To remove excess DNA, the glass slides were vigorously washed with deionized water and dried under nitrogen. Hybridization of dsDNA anchored at the air−glass interface is supported by monitoring the increase of achiral SFG intensity of the vibrational feature ∼2880 cm^{-1}, as previously reported[90] (see the Results and Discussion section).

Dropcast DNA Oligomers on Glass and Quartz. Glass slides or a right-handed Z-cut α-quartz crystal were cleaned in a plasma cleaner (Harrick Plasma, PDC-32G) prior to use. To prepare dsDNA, 200 μM of (D-) or (L-) $(dA)_{12}$ and $(dT)_{12}$ ssDNA with hydroxylated 5′ and 3′ termini (Oligo Synthesis Resource, Yale University) in ddH_2O were mixed in equal volumes, heated in a water bath to 80 °C for 10 min and cooled slowly at room temperature. The $(dA)_{12}$ and $(dT)_{12}$ ssDNA samples were prepared at the same final concentration (100 μM) and subjected to the same heating−cooling process described above. Ten microliters of the solution were applied to the glass or quartz surface. The samples were dried in a desiccator (relative humidity <10%) and immediately measured. Hybridization of dropcast dsDNA is confirmed by attenuated total reflectance-Fourier transform infrared (ATR-FTIR) spectroscopy (Figure S1).

Immobilization of DNA Oligomers at the Air−Water Interface. The $(dA)_{12}$ and $(dT)_{12}$ oligomers were purchased (Oligo Synthesis Resource, Yale University), featuring a 5′ stearyl functionality (Glen Research, Sterling, VA, Cat. No. 10-1979). To prepare dsDNA, the stearyl-$(dA)_{12}$ ssDNA (200 μM) was mixed in equal volume with the complimentary $(dT)_{12}$ ssDNA (200 μM), lacking the 5′ stearyl functionality. Both solutions were prepared in buffer containing 50 mM NaCl, 5 mM KCl, 5 mM $MgCl_2$, 1 mM EDTA, and 10 mM sodium phosphate buffer (pH = 7.2, 4 mM NaH_2PO_4, 6 mM Na_2HPO_4). The solution was heated in a water bath to 80 °C for 10 min and cooled slowly to room temperature. The stearyl-$(dA)_{12}$·$(dT)_{12}$ dsDNA duplex is formed at a final concentration of 100 μM. Hybridization of stearyl-$(dA)_{12}$·$(dT)_{12}$ dsDNA was confirmed by circular dichroism (Figure S2). The dsDNA solution was applied to the air−buffer interface using a Hamilton glass syringe to a final concentration of 50 μM stearyl-$(dA)_{12}$·$(dT)_{12}$ dsDNA.

The obtained stearyl-$(dT)_{12}$ resin did not readily dissolve in 1× buffer and so was dissolved in ddH_2O to a stock concentration of 200 μM. The solution first appeared cloudy but clarified after following the heating protocol detailed above. The stearyl-$(dT)_{12}$ solution (1 mL) in ddH_2O was applied to the air−buffer interface (1.33× salt buffer, 3 mL) to a final concentration of 50 μM.

Stearic acid (>98.5%, Fluka, Cat. No. 85679) was probed by SFG at the air−water interface as a control experiment. Stearic acid visibly precipitates at 50 μM in the buffer (Figure S3). Therefore, the minimal concentration of stearic acid that saturates the air−water interface was determined by the surface adsorption isotherm (Figure S4). Based on the isotherm data, a final stearic acid concentration of 1.75 μM was used to obtain the SFG spectrum of stearic acid at the air−water interface.

Achiral and Chiral Sum Frequency Generation. Achiral SFG spectra were collected using the *ssp* polarization configuration (*s*-polarized sum frequency, *s*-polarized visible, and *p*-polarized IR), and chiral SFG spectra were collected using the *psp* polarization configuration (*p*-polarized sum frequency, *s*-polarized visible, and *p*-

https://doi.org/10.1021/acs.langmuir.2c00365
Langmuir XXXX, XXX, XXX−XXX

polarized IR). The polarization configurations are defined with respect to the laboratory frame (Figure 2).

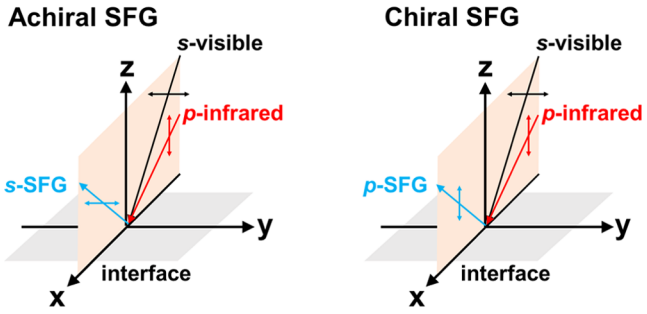

Figure 2. Achiral *ssp* and chiral *psp* polarization configurations used in this study.

The SFG electric field is related to the incident visible and infrared electric fields, E_{VIS} and E_{IR}, and the second-order susceptibility $\chi^{(2)}$

$$E^{I}_{SFG} \propto \sum_{JK} \chi^{(2)}_{IJK} E^{J}_{VIS} E^{K}_{IR} \tag{1}$$

where I, J, and K designates the direction of the respective optical fields (x, y, or z) with respect to the laboratory coordinates and $\chi^{(2)}$ is a 3 × 3 × 3 tensor containing the 27 complex-valued elements, $\chi^{(2)}_{IJK}$. Under the dipole approximation and in the absence of electronic resonance, the achiral and chiral polarization configurations (Figure 2) selectively probe single elements

$$\chi^{(2)}_{ssp} = L_{yy}(\omega_{SFG}) L_{yy}(\omega_{vis}) L_{zz}(\omega_{IR}) \sin \alpha_{IR} \chi^{(2)}_{yyz} \tag{2}$$

$$\chi^{(2)}_{psp} = L_{zz}(\omega_{SFG}) L_{yy}(\omega_{vis}) L_{xx}(\omega_{IR}) \sin \alpha_{SFG} \cos \alpha_{IR} \chi^{(2)}_{zyx} \tag{3}$$

where $\chi^{(2)}_{ssp}$ and $\chi^{(2)}_{psp}$ are the effective second-order susceptibilities, $L(\omega_n)$ is the Fresnel factor at frequency ω_n, and α_n is the angle of the incident and reflected nth laser beam.[13]

Homodyne Sum Frequency Generation. The SFG spectra were collected with a home-built setup previously described.[104] All SFG spectra are collected at 23 ± 0.5 °C and relative humidity <30%. The reported IR frequencies are calibrated using a polystyrene standard (Buck Scientific, East Norwalk, CT, 0.05 mm film). Background spectra were collected by shuttering the IR beam. The background spectra were then subtracted from the SFG intensity spectra. The background-subtracted spectra were normalized to the IR power envelope obtained using a GaAs crystal. The SFG spectra were manually cleaned of cosmic ray intensities.

The intensity spectra were fit to a Lorentzian function that describes the resonant vibrational mode being probed and a contributing nonresonant term

$$I_{SFG} \propto \left| \chi^{(2)}_{NR} + \sum_{q} \frac{A_q}{\omega_{IR} - \omega_q - i\Gamma_q} \right|^2 \tag{4}$$

where I_{SFG} is the intensity of the sum frequency generation, $\chi^{(2)}_{NR}$ is the nonresonant second-order susceptibility, ω_{IR} is the frequency of the IR beam, A_q is the amplitude of the qth resonant vibrational mode, ω_q is the frequency, and Γ_q is the half-width half-maximum.

Heterodyne Sum Frequency Generation. The heterodyne spectra were collected by dropcasting 10 μL of a DNA solution (100 μM in ddH_2O) on the surface of a right-handed Z-cut α-quartz crystal. For every sample, five spectra with an acquisition of 2 min each were collected along both the $+y$ and $-y$ axes of the crystalline quartz. The spectra along each axis were averaged and normalized by the clean quartz surface, as previously described.[17] The imaginary component of the vibrational SFG response was obtained by subtracting the two intensity spectra collected along the $+y$ and $-y$ axes[105]

$$\mathrm{Im}[\chi^{(2)}] = \frac{(I_{+y} - I_{-y})}{4} \tag{5}$$

The heterodyne spectra were fit to the following Lorentzian function

$$\mathrm{Im}[\chi^{(2)}] \propto \mathrm{Im}\left[\sum_{q} \frac{A_q}{\omega_{IR} - \omega_q - i\Gamma_q} \right] \tag{6}$$

RESULTS AND DISCUSSION

Anchor Method: Covalent Attachment of DNA Oligomers on Glass. Scheme 1 presents the methodology for covalent attachment of DNA oligomers to glass (details can be found in the Experimental section).[106] Briefly, a glass slide was washed with hydrochloric acid and then functionalized with APTES ((3-aminopropyl)triethoxysilane) (Step 1, Scheme 1). The amine was then reacted with *para*-azidobenzoic acid through a condensation reaction (Step 2, Scheme 1). The resulting linker azide (Step 3, species I, Scheme 1) was reacted using click chemistry to connect a ssDNA oligo via a DBCO-TEG (dibenzocyclooctyne-triethyleneglycol) functionalization at the ssDNA 5′ end (Step 3, Scheme 1). The DNA-functionalized air−glass interface was washed with water to remove unreacted ssDNA oligo. Using SFG as described in the Experimental section, the glass slides at various steps of the sample preparation were characterized.

Figure 3 shows the achiral SFG (top) and chiral SFG (bottom) spectra obtained using the *ssp* and *psp* polarizations, respectively. The spectral window between 2800 and 3000 cm^{-1} is sensitive to C−H vibrational stretching response (excluding double- or triple-bonded or aromatic C−H groups, which appear above 3000 cm^{-1}).[77,107] Figure 3a shows that the surface linker (Step 3, species I, Scheme 1) gives achiral SFG response, but no chiral SFG response. This linker features three methylene ($-CH_2-$) groups (species I, Scheme 1). Some of these methylene groups are likely oriented on the glass surface and therefore give achiral SFG vibrational signals (Figure 3a, top). However, these methylene groups are achiral and thus are muted in the chiral SFG spectrum (Figure 3a, bottom).

We also obtained the SFG spectra of DBCO-TEG-functionalized $(dA)_{12}$ ssDNA (species II, Scheme 1) at the air−glass interface with (Figure 3b) and without (Figure 3c) vigorous washing with water to remove unreacted ssDNA after Step 3 (Scheme 1). Thus, the achiral spectrum (Figure 3b, top) exhibits spectral features different from just the linker group (Figure 3a, top), suggesting a contribution from the DBCO-TEG-functionalized $(dA)_{12}$ ssDNA, including both bound and unbound ssDNA. The corresponding chiral spectrum exhibits no response (Figure 3b, bottom). Figure 3c presents the achiral and chiral SFG response of DBCO-TEG-functionalized $(dA)_{12}$ ssDNA at the air−glass interface after washing (species II, Scheme 1). Unbound ssDNA has been removed from the sample, and only covalently attached ssDNA remains. As a result, the achiral response changes significantly. However, the sample still yields no chiral SFG response (Figure 3c, bottom).

We also prepared dsDNA samples on the glass surface following the anchor method (Scheme 1) using prehybridized $(dA)_{12}\cdot(dT)_{12}$ dsDNA via the DBCO-TEG functional group on the 5′-end of the $(dA)_{12}$ ssDNA, as shown in Figure 1a. Figure 3d shows the achiral and chiral SFG response of

https://doi.org/10.1021/acs.langmuir.2c00365
Langmuir XXXX, XXX, XXX−XXX

Scheme 1. Anchor Method[a]

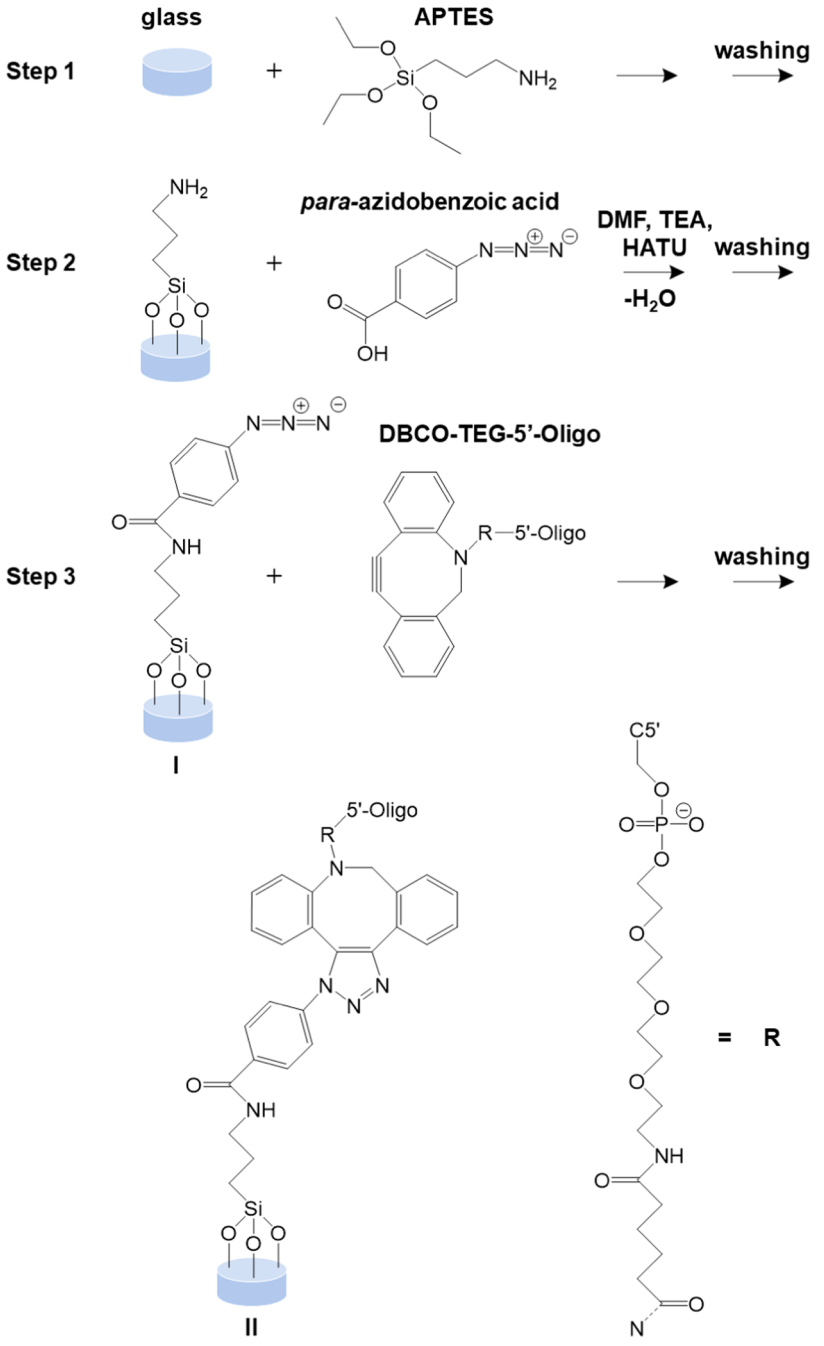

[a]DNA molecules are covalently linked to glass for SFG investigations of ssDNA and dsDNA. Step 1: Functionalization of the glass surface with APTES: (3-aminopropyl)triethoxysilane. Step 2: The amine reacts with *para*-azidobenzoic acid providing surface functionalization with reactive azide for subsequent click chemistry. Step 3: The linker azide was reacted using click chemistry to attach a ssDNA oligo via a DBCO-TEG (dibenzocyclooctyne-triethyleneglycol) group at the ssDNA 5′ end. **R** specifies the chemical structure of the DBCO-TEG connection to the ssDNA 5′ end. DMF: dimethylformamide; TEA: triethylamine; HATU: hexafluorophosphate azabenzotriazole tetramethyl uronium; and DBCO-TEG-oligo: dibenzocyclooctyne-triethyleneglycol-oligo.

DBCO-TEG-functionalized $(dA)_{12}\cdot(dT)_{12}$ dsDNA at the air−glass interface after washing (species II, Scheme 1). Hybridization of dsDNA is supported by the increase in intensity of the vibrational feature ∼2880 cm^{-1} relative to the spectrum of $(dA)_{12}$ ssDNA (Figure 3d). Gibbs-Davis and co-workers observed this same achiral SFG intensity increase upon hybridization of $(dA)_{15}\cdot(dT)_{15}$ dsDNA anchored at the silica−buffer interface.[90] Among all of the samples, only the $(dA)_{12}\cdot(dT)_{12}$ dsDNA gives chiral SFG response (Figure 3).

The results demonstrate that the anchor method when combined with achiral and chiral SFG to probe C−H stretching modes can be used for characterization and quality control during sample preparation. Importantly, the results support that the anchor method combined with chiral SFG can be used for background-free, facile detection of DNA hybridization on glass surfaces.

Island Method: Dropcast DNA Oligomers on Glass and Quartz. We used the island method to prepare hydrated

https://doi.org/10.1021/acs.langmuir.2c00365
Langmuir XXXX, XXX, XXX−XXX

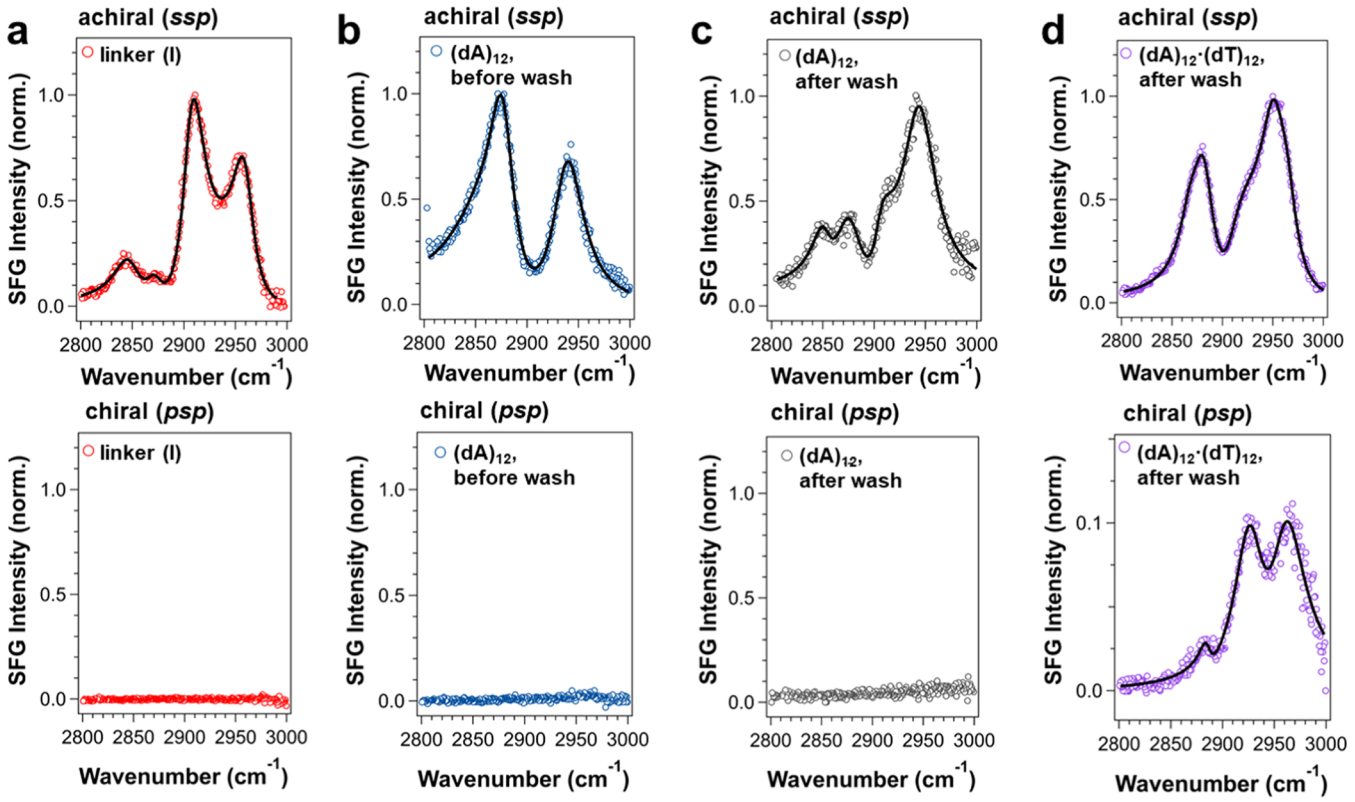

Figure 3. Achiral (*ssp*) and chiral (*psp*) SFG spectra in the C−H stretch region of the glass surface during various steps of sample preparation using the "anchor" method (Scheme 1). (a) Covalent linker molecule before conjugation with DBCO-TEG-functionalized DNA (species I, Scheme 1). (b) After conjugation of $(dA)_{12}$ ssDNA, but without washing with water to remove unreacted ssDNA (species II, Scheme 1). (c) After washing away unreacted $(dA)_{12}$ ssDNA (species II, Scheme 1). (d) After conjugation of dsDNA and after washing of unbound $(dA)_{12}\cdot(dT)_{12}$ dsDNA (species II, Scheme 1). Acquisition time is 15 min (*ssp*) and 25 min (*psp*) for each spectrum. Within (a−d), *ssp* and *psp* spectra are normalized to the highest intensity *ssp* feature, so that *ssp* (top) and *psp* (bottom) intensities can be directly compared; however, intensities are not comparable across figures.

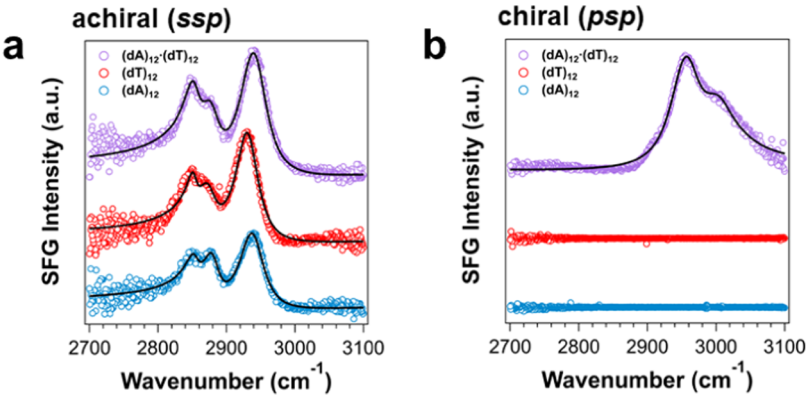

Figure 4. (a) Achiral (*ssp*) and (b) chiral (*psp*) SFG spectra of 100 μM $(dA)_{12}$ and $(dT)_{12}$ ssDNA, and $(dA)_{12}\cdot(dT)_{12}$ dsDNA dropcast at the air−glass interface in the C−H stretching region. Acquisition time is 15 min for all spectra. The spectra are shown with offsets. a.u.: arbitrary units.

thin films of ssDNA and dsDNA samples on glass slides and obtained the SFG spectra (Figure 4). The dsDNA sample was prepared by combining $(dA)_{12}$ and $(dT)_{12}$ ssDNA in a 1:1 mixture in ddH_2O, followed by heating at 80 °C for 10 min, and slowly cooling the solution to room temperature (see Methods). The solution was dried on glass in the presence of desiccant. Hybridization of dsDNA in films was confirmed by ATR-FTIR spectroscopy (Figure S1).[73,74,77,108] Figure 4a shows the achiral SFG spectra in the C−H stretching region (2700−3100 cm^{-1}) for single-stranded $(dA)_{12}$ in blue, single-stranded $(dT)_{12}$ in red, and double-stranded $(dA)_{12}\cdot(dT)_{12}$ in purple. The achiral spectra show only subtle differences between the SFG responses of ssDNA and dsDNA, consistent with prior reports by Geiger and co-workers.[89] Figure 4b shows the chiral SFG spectra in the same spectral window. The two single-stranded $(dA)_{12}$ and $(dT)_{12}$ samples give no chiral SFG response (Figure 4b, red and blue). Only the double-stranded $(dA)_{12}\cdot(dT)_{12}$ shows a strong chiral SFG signal (Figure 4b, purple). The results again illustrate that chiral SFG is muted to the local chiral centers along the DNA backbone but highly sensitive to the macroscopic chirality exhibited by double-helix dsDNA. Thus, the preparation of DNA on glass

https://doi.org/10.1021/acs.langmuir.2c00365
Langmuir XXXX, XXX, XXX−XXX

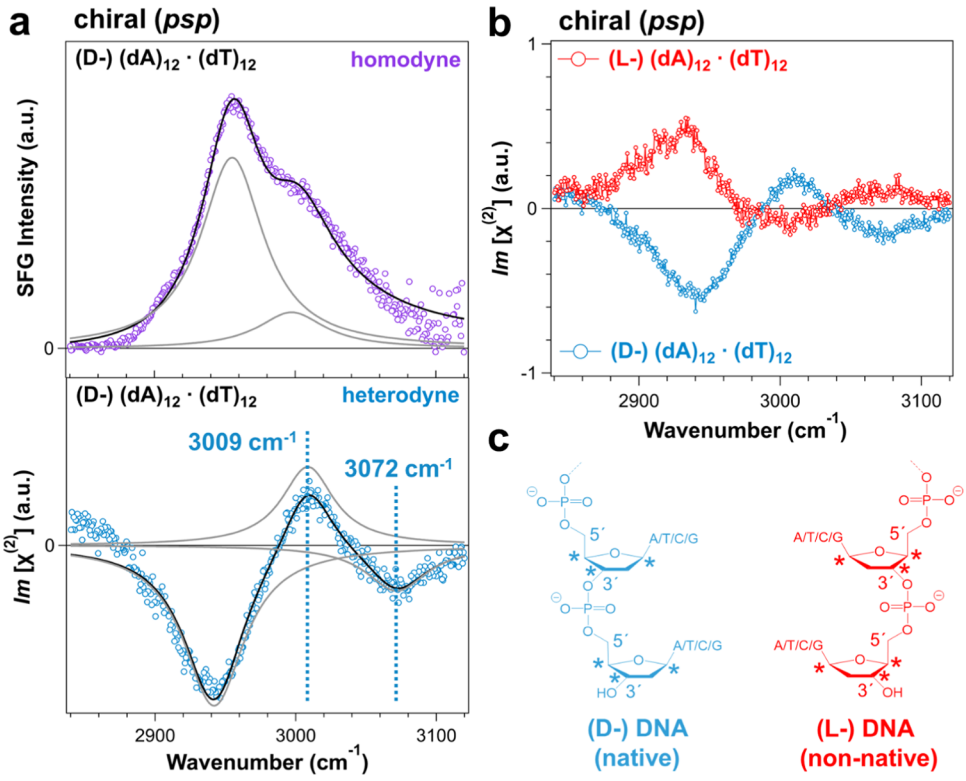

Figure 5. Chiral (*psp*) SFG spectra in the C−H stretching region of 100 μM $(dA)_{12}\cdot(dT)_{12}$ dsDNA dropcast at the air−glass and air−quartz interfaces. (a) Homodyne (purple) versus heterodyne (blue) chiral SFG spectra of (D-) $(dA)_{12}\cdot(dT)_{12}$ dsDNA on glass (purple) versus quartz (blue), respectively. Component peaks are shown as gray lines. Fitting parameters are given in Table S1. (b) Heterodyne phase-resolved chiral SFG spectra of (L-) and (D-) $(dA)_{12}\cdot(dT)_{12}$ dsDNA on quartz. Homodyne acquisition time is 15 min. Heterodyne acquisition time is 20 min. a.u.: arbitrary units. (c) Chemical structures of the sugar-phosphate backbone of native (D-) DNA versus non-native (L-) DNA.

using the island method for chiral SFG characterization also provides a straightforward method for background-free, label-free detection of DNA double-helix structures.

Figure 4 includes the spectral region of 3000−3100 cm^{-1}. This high-frequency spectral window encompasses the aromatic C−H stretching modes associated with the adenine and thymine nucleobases (see structures in Figure 1d).[74,108−114] The achiral SFG spectra (Figure 4a) show negligible response above 3000 cm^{-1} regardless of the hybridization state of the DNA molecules. However, the chiral spectrum of dsDNA (Figure 4b, purple) exhibits strong C−H stretching signals above 3000 cm^{-1}. Upon hybridization, the base-paired nucleobases are expected to follow the double-helix structure, stacking into a macroscopic chiral architecture, thereby becoming chiral SFG active. These aromatic C−H stretching bands from the nucleobases are analyzed together with the heterodyne SFG results (see below). The observation of these bands reveals a promising application of chiral SFG for probing highly specific vibrational structures of the aromatic rings in the nucleobases of dsDNA.

Dropcasting DNA on glass allows only for the collection of the homodyne SFG response, which is proportional to the square of the second-order susceptibility tensor $\chi^{(2)}$ (see the Experimental section).[13] However, $\chi^{(2)}$ is a complex-valued tensor containing real and imaginary parts.[105] To isolate the imaginary component of $\chi^{(2)}$ (i.e., $\mathrm{Im}[\chi^{(2)}]$) and resolve the phase of individual vibrational resonances, a heterodyne approach is needed. This can be accomplished by dropcasting DNA on the surface of a quartz crystal that produces a strong SFG response and provides a phase reference (see the Experimental section).[17,115,116]

Figure 5a presents the heterodyne chiral SFG spectrum (blue) from 2840 to 3120 cm^{-1} of $(dA)_{12}\cdot(dT)_{12}$ dsDNA dropcast at the air−quartz interface. The homodyne chiral SFG spectrum (purple) is also included for comparison (Figure 5a, purple). While the homodyne response is positive-valued, the heterodyne response contains phase information and appears as positive or negative peaks in the spectrum (Figure 5a). The phase information allows for resolving vibrational features in the heterodyne spectrum that are hidden in the homodyne spectrum. Of importance are the aromatic C−H stretching bands at 3000−3100 cm^{-1} that have been identified in the homodyne spectra (Figure 4b and also Figure 5a, purple). The homodyne response (Figure 5a, purple) appears as a broad shoulder band, whereas the heterodyne spectrum (Figure 5a, blue) shows two vibrational bands with a positive band at 3009 ± 1 and a negative peak at 3072 ± 2 cm^{-1} (see Figure 5a, blue and Table S1). There are only three aromatic C−H moieties in a (dA)·(dT) dsDNA base pair. They include C6-H of thymine and C2-H and C8-H of adenine (see Figure 1d for atom numbering). Based on previous Raman and infrared studies,[109−114] the higher-frequency peak (3072 cm^{-1}) can be due to C6-H of thymine and the lower-frequency peak (3009 cm^{-1}) is likely due to C8-H and/or C2-H of adenine. Although these spectral features are not crucial in sensing DNA double helices, they could be extremely useful in probing highly specific local structures. This capability shows the promise of further developing the chiral SFG approach to study conformational and dynamical changes of DNA in response

https://doi.org/10.1021/acs.langmuir.2c00365
Langmuir XXXX, XXX, XXX−XXX

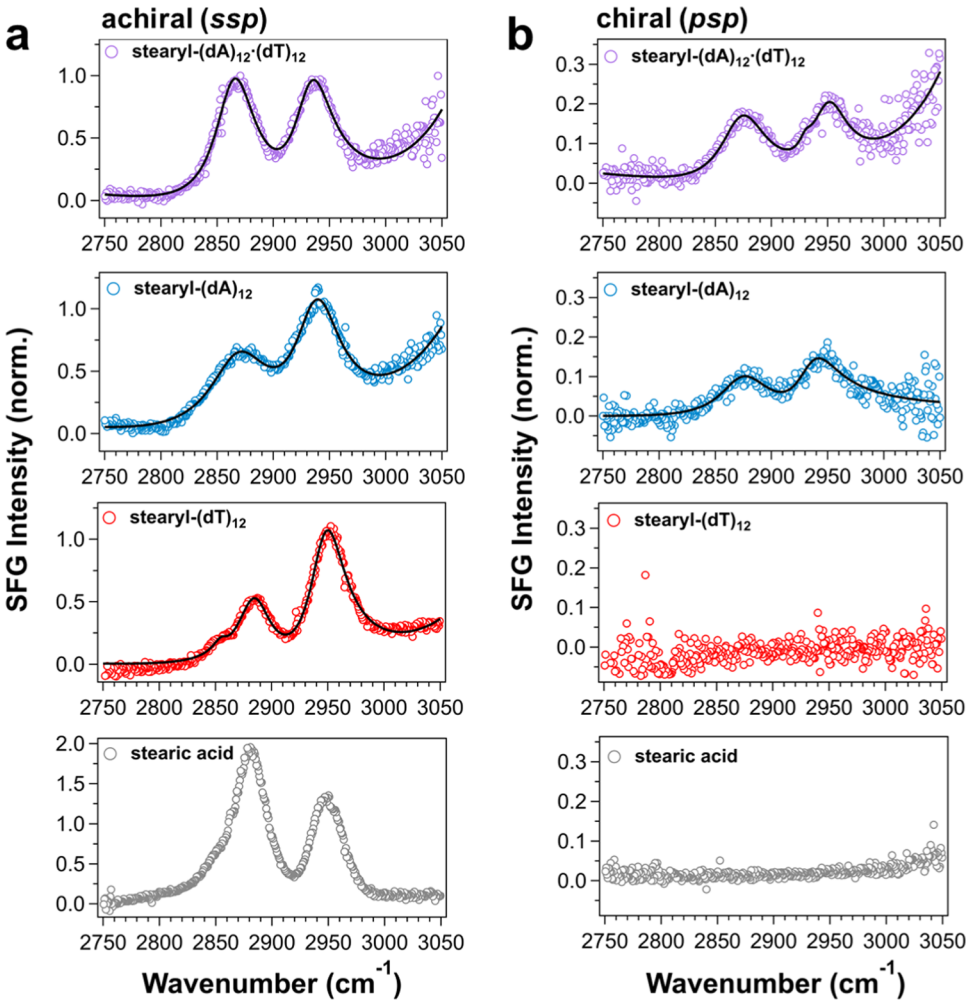

Figure 6. Achiral (*ssp*) and chiral (*psp*) SFG spectra in the C−H stretching region of 50 μM stearyl-$(dA)_{12}$·$(dT)_{12}$ dsDNA, stearyl-$(dA)_{12}$, stearyl-$(dT)_{12}$, and 1.75 μM stearic acid at the air−water interface. All DNA constructs were measured in buffer (see the Experimental section). Stearic acid was measured in water. (a) All constructs show an achiral SFG response. (b) Chiral SFG response from stearyl-$(dA)_{12}$·$(dT)_{12}$ dsDNA, stearyl-$(dA)_{12}$, stearyl-$(dT)_{12}$, and stearic acid. Acquisition time is 25 min for all spectra; stearyl-$(dA)_{12}$·$(dT)_{12}$ dsDNA chiral (*psp*) SFG spectrum is an average of four spectra. All spectra are normalized to the feature ~2870 cm^{-1} in the achiral (*ssp*) spectrum of stearyl-$(dA)_{12}$·$(dT)_{12}$ dsDNA, so that all spectral intensities can be directly compared.

to perturbations, such as photoexcitation, or molecular interactions with bioactive molecules, including proteins and drugs.

Another application of the heterodyne chiral SFG approach for DNA sensing is that enantiomeric native (D-) dsDNA and non-native (L-) dsDNA are expected to give chiral SFG response with opposite phases, as in our previous observation for enantiomeric protein secondary structures formed by native (L-) and non-native (D-) proteins.[17] However, the vibrational SFG responses of DNA enantiomers have never been compared. Figure 5b compares the heterodyne chiral SFG spectra of (D-) dsDNA and (L-) dsDNA. The spectra show mirror-image chiral SFG responses in opposite phases. Because ssDNA molecules give no chiral SFG signals (Figure 4b), the opposite signs of the chiral SFG response must arise from the macroscopic right-handed double helix formed by native (D-) dsDNA versus the macroscopic left-handed double helix formed by the non-native enantiomer (L-) dsDNA. This finding again demonstrates chiral SFG is not sensitive to the local chiral centers along the DNA backbone (Figure 5c), but the macroscopic chirality of the dsDNA double helix, as predicted by chiral SFG theory.[50] The chiral SFG results of this enantiomeric dsDNA pair illustrate the remarkable sensitivity and utility of heterodyne chiral SFG to differentiate the absolute macroscopic chirality of dsDNA double-helix structures.

Buoy Method: Immobilization of DNA Oligomers at the Air−Water Interface. We employ a hydrophobic alkyl chain as a molecular "buoy" to localize DNA at the air−water interface for SFG studies (Figure 1c). Figure 6 presents the results for dsDNA and ssDNA together with control experiments. A stearyl moiety is linked to the two ssDNAs at the 5′ end and to dsDNA at the 5′ end of the $(dA)_{12}$ strand (Figure 1c). The 5′ stearyl functionalization does not inhibit hybridization in forming a double-helix structure, as confirmed by circular dichroism spectroscopy (Figure S2).[117] A control experiment with stearic acid alone produces an achiral SFG response as previously reported (Figure 6a, gray).[118] However, stearic acid alone does not produce chiral SFG response (Figure 6b, gray). Stearyl-$(dT)_{12}$ (Figure 6, red) produces an achiral response, but not a chiral response, consistent with our observations of ssDNA immobilized at the air−glass interface (Figures 3 and 4). Stearyl-$(dA)_{12}$·$(dT)_{12}$ dsDNA gives not only

https://doi.org/10.1021/acs.langmuir.2c00365
Langmuir XXXX, XXX, XXX−XXX

achiral response but also chiral SFG response as expected for formation of the double helix (Figure 6, purple).

To our surprise, stearyl-$(dA)_{12}$ at the air−water interface generates not only achiral but also chiral SFG response (Figure 6, blue). This was unexpected given that ssDNA that lacks macroscopic chirality and therefore should not produce a chiral SFG response (Figures 3 and 4). Looking into the literature, we found that poly(dA) can form parallel double-helix dsDNA (see the Results and Discussion section).[97,101−103] Indeed, this type of parallel poly(dA)·poly(dA) duplex formation has been observed for simple RNA[94,95] as well as DNA oligomers,[96−103] where the adenine−adenine base pairing (Figure 7) adopts the

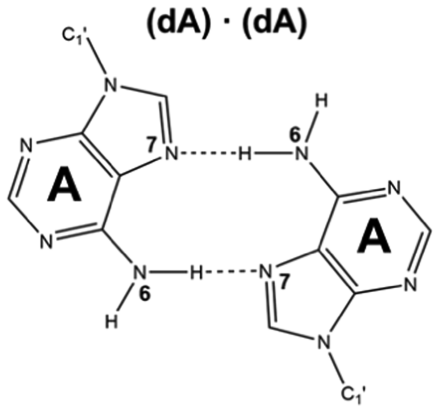

Figure 7. Homo (dA)·(dA) base pairing in parallel dsDNA featuring N6-H···N7 hydrogen bonds.

type I hydrogen-bonding configuration, as shown in Figure 7. To further validate the formation of the parallel duplex, we examined the effect of salt. We found that the chiral SFG response of stearyl-$(dA)_{12}$ at the air−water interface (Figure 6b, blue) was not observed in the absence of salt in the buffer (Figure S5). Because salt is needed to stabilize the parallel duplex,[94,95] removing salt from the buffer should destabilize the duplex at the air−water interface and lead to null chiral SFG response.

Intriguingly, the $(dA)_{12}$ ssDNA sample only gives a chiral SFG response when prepared using the buoy method (Figure 6b), but not the anchor and island methods (Figures 3 and 4). The buoy method is different from the other two methods because the buoy stearyl groups not only localize but also orient the $(dA)_{12}$ ssDNA strands at the air−water interface. Unlike the anchor method, the buoy method allows the ssDNA strands to freely diffuse in the surface region. Because the buoy stearyl group is attached to the 5′ end of the ssDNA, each $(dA)_{12}$ ssDNA molecule is oriented with the 5′ end near the surface and the 3′ end extending to the bulk. We expect that this parallel alignment of $(dA)_{12}$ at the interface, together with strong base stacking interactions of adenine compared to thymine,[99] as well as interfacial crowding,[119] can facilitate the interstrand type I hydrogen-bonding configuration for the adenine−adenine base pairing (Figure 7). Hence, parallel $(dA)_{12}$·$(dA)_{12}$ double helix is favored at the air−water interface, thereby giving the chiral SFG signals (Figure 6b, blue).

In general, the results presented in Figure 6 demonstrate that the "buoy" method can be successfully used to localize DNA at the air−water interface. With this approach, chiral SFG detects the macroscopic chirality of the dsDNA double helix in aqueous environments.

Implications. Immobilization of ssDNA and dsDNA at interfaces is relevant to fundamental biophysical questions and crucial to a diverse range of biotechnological applications. However, an understanding of the influence of the interface on the structure of immobilized DNA is required. Few techniques offer the capability to study the structures of biomacromolecules at interfaces. Achiral vibrational SFG is nonlinear vibrational spectroscopy that is interface selective, *in situ*, and sensitive to the orientations of molecules at interfaces. In addition, chiral vibrational SFG is sensitive to macroscopic chirality of biomacromolecules, such as the handedness of the dsDNA double helix, and can readily distinguish enantiomers. These properties make SFG a powerful technology for understanding how the interface impacts the structures of biomacromolecules. Vibrational resonances offer a direct readout of the chemical environment and molecular structure. Chiral SFG combined with the various interfacial preparatory platforms presented here (the "anchor", "island", and "buoy" methods, Figure 1) represents a versatile and highly sensitive approach for detecting chiral DNA secondary structures at interfaces.

Use of a molecular "anchor" to covalently attach ssDNA and dsDNA on glass will offer SFG researchers the versatility to study DNA at both the air−glass and water−glass interfaces (Figures 1a and 3). Indeed, anchoring methodologies were fruitfully utilized in prior SFG studies by several groups.[53,54,88−90,120−122] Covalent attachment of DNA to a glass substrate has found application in the construction of DNA biosensors.[123,124] However, different linker chemistry could make variable contributions to the achiral SFG vibrational response, since SFG is sensitive to the identities of functional groups as well as molecular orientation at the interface. Therefore, the use of novel linkers for anchoring DNA on a solid substrate will require benchmarking the SFG vibrational response. Nonetheless, chiral SFG is silent to the linker structures so long as the structures are achiral, simplifying the interpretation of vibrational spectra.

Dropcasting DNA "islands" on glass (or quartz) substrates (Figures 1b, 4, and 5) is straightforward and less labor intensive than covalent attachment to glass. In the absence of any molecular anchor, researchers can trust that DNA alone contributes to the SFG signal. One drawback is that dropcasting DNA does not offer the option for *in situ* studies at aqueous interfaces. A quartz crystal substrate can be utilized for heterodyne studies of dropcast DNA (Figure 5). This approach resolves the phase of the SFG absorbance, revealing additional details about the vibrational response of the DNA compared to homodyne approaches (Figure 5a). For example, we clearly observe at least two C−H stretching vibrations with opposite phase in the region 3000−3100 cm^{-1} specific to the adenine and thymine nucleobases (Figure 5a, blue), which may provide sensitive markers for nucleobase structure and chemical environment. Therefore, dropcasting DNA can potentially provide fingerprints for rapid qualitative screening of DNA secondary structures and the chirality of molecular enantiomers (Figure 5b).

This work has also introduced the use of a molecular "buoy" for characterizing DNA at the air−water interface (Figures 1c and 6). This buoy method was previously applied for SFG studies of protein[125] but has not been used to study DNA with SFG. Our molecular constructs utilize a stearyl (C_{18}) moiety

https://doi.org/10.1021/acs.langmuir.2c00365
Langmuir XXXX, XXX, XXX−XXX

attached at the 5′ end of one DNA strand to "buoy" DNA at the air−water interface. Chiral SFG detects the double-helix structure of not only the canonical antiparallel $(dA)_{12}\cdot(dT)_{12}$ double helix but also the noncanonical parallel $(dA)_{12}\cdot(dA)_{12}$ double helix at the air−water interface (Figure 6b). This platform offers researchers the capability to use SFG to probe DNA confirmation in aqueous solutions, where researchers can easily control temperature, electrolyte concentrations, pH, or DNA binding partners. Therefore, the buoy technique should be amenable to *in situ* studies including biochemical kinetics and DNA conformational changes. The buoy method when combined with advanced SFG approaches (e.g., external heterodyne SFG, two-dimensional SFG, and time-resolved pump-probe SFG) could be useful in attacking fundamental problems related to the structures and dynamics of DNA at interfaces, including solvation dynamics and vibrational energy-transfer relaxation upon photoexcitation.

Despite the promise of SFG for the study of DNA at interfaces, only a few major reports have emerged in the past 15 years.[53,54,88−90,120−122,126,127] For example, Geiger and co-workers monitored the asymmetric stretching of thymine $-CH_3$ (Figure 1d) in $(dA)_{15}\cdot(dT)_{15}$ oligos anchored on glass and demonstrated that chiral SFG can distinguish the directionality of the thymine strand relative to the air−glass interface.[88] The Bonn and Tahara groups applied homodyne and heterodyne achiral SFG to monitor how interactions between DNA and lipids restructure and reorient water at the air−water interface.[126,127] Petersen and co-workers used chiral SFG at the water−glass interface to report the first all-optical observation of the O−H stretching of water molecules in the "spine of hydration" in the minor groove of anchored DNA.[122] Koelsch and co-workers examined the achiral SFG response in the C−H and C═O stretching regions of ssDNA immobilized on gold using a thiol anchor[54] and observed strong dependences of the achiral SFG response on factors, such as ssDNA orientation, the presence of an air or liquid interface, or even the identity of the liquid (e.g., PBS buffer or D_2O). Recently, Gibbs-Davis and co-workers identified achiral SFG vibrational signatures of temperature-induced melting of $(dA)_{15}\cdot(dT)_{15}$ dsDNA oligos anchored at the glass−buffer interface,[90] demonstrating that achiral SFG can distinguish ssDNA from dsDNA at an interface by studying various C−H stretching modes through detailed analysis of the relative intensities of various vibrational bands.

While achiral SFG has been used to distinguish ssDNA from dsDNA,[88−90] systematic comparisons of chiral and achiral SFG spectra of ssDNA versus dsDNA were not previously reported. Our analyses using three different sample preparatory platforms (Figures 3, 4, and 6) show that chiral SFG is muted to ssDNA but provide strong signals in the C−H stretching regions for double-helix DNA structures. Thus, chiral SFG offers a background-free, label-free, and straightforward method to distinguish dsDNA from ssDNA. Achiral SFG, like infrared spectroscopy (Figure S1), requires researchers to compare differences between relative vibrational intensities to distinguish dsDNA from ssDNA. The simplicity of the chiral SFG response (0 = ssDNA, 1 = dsDNA) is key and can potentially support the development of high-throughput technologies for label-free detection of dsDNA hybridization.

The capability of chiral SFG to distinguish dsDNA from ssDNA (Figures 3, 4, and 6) and of phase-resolved chiral SFG to distinguish right-handed (D-) versus left-handed (L-) dsDNA (Figure 5) illustrates that chiral SFG is sensitive to the macroscopic chirality[128] of the dsDNA double-helix secondary structure but not local chiral chemical centers in ssDNA. Our group previously demonstrated that chiral SFG distinguishes well-defined secondary structures of proteins (e.g., β-sheet and α-helix) from disordered structures that give no SFG response.[13,19,125] Similar to disordered protein, interfacial ssDNA lacks a stable secondary structure resulting in null chiral SFG response in all cases (Figures 3, 4, and 6). Our detection of poly-adenine parallel double-helix formation (Figure 6b, blue) is the first observation with chiral SFG of a noncanonical antiparallel double-helix DNA secondary structure. The capability of chiral SFG to detect both canonical and noncanonical helicity of dsDNA illustrates the promise of chiral SFG in characterizing DNA secondary structures.

CONCLUSIONS

The three immobilization methodologies presented here set the stage for a wide range of future SFG investigations. Our work has demonstrated that the three immobilization methodologies (Figure 1) can be broadly useful in revealing new applications of chiral SFG. These potential new applications include (1) background-free, label-free detection of DNA hybridization, (2) differentiation of DNA double helices in opposite handedness, (3) observation of noncanonical DNA secondary structures, and (4) characterization of specific local vibrational structures of nucleobases. The immobilization methodologies will also be useful for other researchers to explore numerous variables that can impact the structure of DNA at solid−air, solid−liquid, and air−liquid interfaces. These variables may include electrolyte concentrations, binding, and interactions of DNA with proteins or small molecules, as well as crowding effects on DNA folding.

Further development of the SFG methods for probing DNA demands not only experimental exploration but also advances in theoretical and computational approaches. On the one hand, the SFG field has witnessed fast-moving developments of computational methods in modeling achiral SFG responses from plain air−water interfaces and charged water interfaces, for example, using *ab initio*[129] or electric field mapping methods.[17,18,130−134] The parallel development of DNA systems is challenging due to the increasing complexity of biomacromolecular structures. Hence, experimental benchmarks will be critical to validate novel computational approaches. The platforms developed here will be useful for providing the necessary benchmarks for direct comparison with computation when probing the structural dynamics, solvation, and photochemistry of DNA. Experiments can also validate SFG response as a function of DNA concentration, length, sequence, orientation, and chirality at various interfaces using different polarization settings.[89] These experimental results will aid the implementation of theoretical approaches for modeling the SFG response of DNA,[121] toward the fundamental understanding of molecular behaviors of DNA at interfaces. The three preparatory platforms presented here will be useful for future experimental and computational investigations of SFG vibrational response of DNA molecules at interfaces.

Our work demonstrates the sensitivity of chiral SFG to double-helix formation at interfaces, which is expected to enable numerous technological applications, including the development of novel DNA nanosensors, as well as new means for detecting DNA structure and hybridization *in vivo*.

https://doi.org/10.1021/acs.langmuir.2c00365
Langmuir XXXX, XXX, XXX−XXX

■ ASSOCIATED CONTENT

Supporting Information

The Supporting Information is available free of charge at https://pubs.acs.org/doi/10.1021/acs.langmuir.2c00365.

ATR-FTIR of dsDNA and ssDNA films; circular dichroism of stearyl-dsDNA and ssDNA solutions; precipitation of stearic acid at the air−water interface; adsorption isotherm of stearic acid at the air−water interface; fitting parameters for homodyne and heterodyne spectra of dsDNA films; achiral and chiral SFG spectra of stearyl-$(dA)_{12}$ at the air−water interface in the absence of salt buffer; and chiral SFG spectrum of a plain glass slide (PDF)

■ AUTHOR INFORMATION

Corresponding Author

Elsa C. Y. Yan − *Department of Chemistry, Yale University, New Haven, Connecticut 06520, United States;* orcid.org/0000-0002-3583-1627; Email: elsa.yan@yale.edu

Authors

Ethan A. Perets − *Department of Chemistry, Yale University, New Haven, Connecticut 06520, United States;* orcid.org/0000-0001-9554-776X

Kristian B. Olesen − *Department of Chemistry, Yale University, New Haven, Connecticut 06520, United States*

Complete contact information is available at: https://pubs.acs.org/10.1021/acs.langmuir.2c00365

Notes

The authors declare no competing financial interest.

■ ACKNOWLEDGMENTS

The authors acknowledge Dr. Jacob Black (Yale University), Dr. Pablo E. Videla (Yale University), Daniel Konstantinovsky (Yale University), and Prof. Chenxiang Lin (Yale University) for helpful discussions. The authors thank Sarah Ostresh (Yale University) for generating the TOC graphic. E.A.P. was supported by the NIH (5T32GM008283-31) and a John C. Tully Chemistry Research Fellowship. E.C.Y.Y. acknowledges NSF support (CHE 1905169).

■ REFERENCES

(1) Watson, J. D.; Crick, F. H. Molecular structure of nucleic acids: a structure for deoxyribose nucleic acid. *Nature* **1953**, *171*, 737−738.

(2) SantaLucia, J.; Hicks, D. The Thermodynamics of DNA Structural Motifs. *Annu. Rev. Biophys. Biomol. Struct.* **2004**, *33*, 415−440.

(3) Kuriyan, J.; Konforti, B.; Wemmer, D. *The Molecules of Life: Physical and Chemical Principles*; WW Norton & Company, 2012.

(4) Herbert, A.; Lowenhaupt, K.; Spitzner, J.; Rich, A. Chicken double-stranded RNA adenosine deaminase has apparent specificity for Z-DNA. *Proc. Natl. Acad. Sci. U.S.A.* **1995**, *92*, 7550.

(5) Bochman, M. L.; Paeschke, K.; Zakian, V. A. DNA secondary structures: stability and function of G-quadruplex structures. *Nat. Rev. Genet.* **2012**, *13*, 770−780.

(6) Varshney, D.; Spiegel, J.; Zyner, K.; Tannahill, D.; Balasubramanian, S. The regulation and functions of DNA and RNA G-quadruplexes. *Nat. Rev. Mol. Cell Biol.* **2020**, *21*, 459−474.

(7) Fleming, A. M.; Stewart, K. M.; Eyring, G. M.; Ball, T. E.; Burrows, C. J. Unraveling the 4 n− 1 rule for DNA i-motif stability: base pairs vs. loop lengths. *Org. Biomol. Chem.* **2018**, *16*, 4537−4546.

(8) Murat, P.; Zhong, J.; Lekieffre, L.; Cowieson, N. P.; Clancy, J. L.; Preiss, T.; Balasubramanian, S.; Khanna, R.; Tellam, J. G-quadruplexes regulate Epstein-Barr virus−encoded nuclear antigen 1 mRNA translation. *Nat. Chem. Biol.* **2014**, *10*, 358−364.

(9) Shen, J.; Varshney, D.; Simeone, A.; Zhang, X.; Adhikari, S.; Tannahill, D.; Balasubramanian, S. Promoter G-quadruplex folding precedes transcription and is controlled by chromatin. *Genome Biol.* **2021**, *22*, 143.

(10) Fleming, A. M.; Zhou, J.; Wallace, S. S.; Burrows, C. J. A role for the fifth G-track in G-quadruplex forming oncogene promoter sequences during oxidative stress: Do these "spare tires" have an evolved function? *ACS Cent. Sci.* **2015**, *1*, 226−233.

(11) Herbert, A. ADAR and Immune Silencing in Cancer. *Trends Cancer* **2019**, *5*, 272−282.

(12) Wang, J.; Chen, X.; Clarke, M. L.; Chen, Z. Detection of chiral sum frequency generation vibrational spectra of proteins and peptides at interfaces in situ. *Proc. Natl. Acad. Sci. U.S.A.* **2005**, *102*, 4978.

(13) Yan, E. C. Y.; Fu, L.; Wang, Z.; Liu, W. Biological Macromolecules at Interfaces Probed by Chiral Vibrational Sum Frequency Generation Spectroscopy. *Chem. Rev.* **2014**, *114*, 8471−8498.

(14) Perets, E. A.; Yan, E. C. Y. The H2O Helix: The Chiral Water Superstructure Surrounding DNA. *ACS Cent. Sci.* **2017**, *3*, 683−685.

(15) Perets, E. A.; Videla, P. E.; Yan, E. C. Y.; Batista, V. S. Chiral Inversion of Amino Acids in Antiparallel β-Sheets at Interfaces Probed by Vibrational Sum Frequency Generation Spectroscopy. *J. Phys. Chem. B* **2019**, *123*, 5769−5781.

(16) Perets, E. A.; Yan, E. C. Y. Chiral Water Superstructures around Antiparallel β-Sheets Observed by Chiral Vibrational Sum Frequency Generation Spectroscopy. *J. Phys. Chem. Lett.* **2019**, *10*, 3395−3401.

(17) Perets, E. A.; Konstantinovsky, D.; Fu, L.; Chen, J.; Wang, H.-F.; Hammes-Schiffer, S.; Yan, E. C. Y. Mirror-image antiparallel β-sheets organize water molecules into superstructures of opposite chirality. *Proc. Natl. Acad. Sci. U.S.A.* **2020**, *117*, 32902.

(18) Konstantinovsky, D.; Perets, E. A.; Yan, E. C. Y.; Hammes-Schiffer, S. Simulation of the Chiral Sum Frequency Generation Response of Supramolecular Structures Requires Vibrational Couplings. *J. Phys. Chem. B* **2021**, *125*, 12072−12081.

(19) Fu, L.; Liu, J.; Yan, E. C. Y. Chiral Sum Frequency Generation Spectroscopy for Characterizing Protein Secondary Structures at Interfaces. *J. Am. Chem. Soc.* **2011**, *133*, 8094−8097.

(20) Fu, L.; Wang, Z.; Yan, E. C. Y. Chiral Vibrational Structures of Proteins at Interfaces Probed by Sum Frequency Generation Spectroscopy. *Int. J. Mol. Sci.* **2011**, *12*, 9404−9425.

(21) Wang, Z.; Fu, L.; Ma, G.; Yan, E. C. Y. Broad-Bandwidth Chiral Sum Frequency Generation Spectroscopy for Probing the Kinetics of Proteins at Interfaces. *Langmuir* **2015**, *31*, 11384−11398.

(22) Hosseinpour, S.; Roeters, S. J.; Bonn, M.; Peukert, W.; Woutersen, S.; Weidner, T. Structure and dynamics of interfacial peptides and proteins from vibrational sum-frequency generation spectroscopy. *Chem. Rev.* **2020**, *120*, 3420−3465.

(23) Arnott, S.; Selsing, E. Structures for the polynucleotide complexes poly(dA) · poly(dT) and poly(dT) · poly(dA) · poly(dT). *J. Mol. Biol.* **1974**, *88*, 509−521.

(24) Kopka, M. L.; Fratini, A. V.; Drew, H. R.; Dickerson, R. E. Ordered water structure around a B-DNA dodecamer: A quantitative study. *J. Mol. Biol.* **1983**, *163*, 129−146.

(25) Arnott, S.; Chandrasekaran, R.; Hall, I.; Puigjaner, L.; Walker, J.; Wang, M. DNA Secondary Structures: Helices, Wrinkles, and Junctions. In *Cold Spring Harbor Symposia on Quantitative Biology*; Cold Spring Harbor Laboratory Press, 1983; pp 53−65.

(26) Nelson, H. C. M.; Finch, J. T.; Luisi, B. F.; Klug, A. The structure of an oligo (dA) · oligo (dT) tract and its biological implications. *Nature* **1987**, *330*, 221−226.

(27) Park, H.-S.; Arnott, S.; Chandrasekaran, R.; Millane, R.; Campagnari, F. Structure of the α-form of poly [d (A)] · poly [d (T)] and related polynucleotide duplexes. *J. Mol. Biol.* **1987**, *197*, 513−523.

(28) DiGabriele, A. D.; Sanderson, M. R.; Steitz, T. A. Crystal lattice packing is important in determining the bend of a DNA dodecamer containing an adenine tract. *Proc. Natl. Acad. Sci. U.S.A.* **1989**, *86*, 1816−1820.

(29) Kondo, J.; Adachi, W.; Umeda, S.; Sunami, T.; Takénaka, A. Crystal structures of a DNA octaplex with I-motif of G-quartets and its splitting into two quadruplexes suggest a folding mechanism of eight tandem repeats. *Nucleic Acids Res.* **2004**, *32*, 2541−2549.
(30) Burge, S.; Parkinson, G. N.; Hazel, P.; Todd, A. K.; Neidle, S. Quadruplex DNA: sequence, topology and structure. *Nucleic Acids Res.* **2006**, *34*, 5402−5415.
(31) Behling, R. W.; Kearns, D. R. Proton two-dimensional nuclear Overhauser effect and relaxation studies of poly (dA) · poly (dT). *Biochemistry* **1986**, *25*, 3335−3346.
(32) Liepinsh, E.; Otting, G.; Wüthrich, K. NMR observation of individual molecules of hydration water bound to DNA duplexes: direct evidence for a spine of hydration water present in aqueous solution. *Nucleic Acids Res.* **1992**, *20*, 6549−6553.
(33) Williamson, J. R. G-quartet structures in telomeric DNA. *Annu. Rev. Biophys. Biomol. Struct.* **1994**, *23*, 703−730.
(34) Hud, N. V.; Smith, F. W.; Anet, F. A.; Feigon, J. The selectivity for K+ versus Na+ in DNA quadruplexes is dominated by relative free energies of hydration: a thermodynamic analysis by 1H NMR. *Biochemistry* **1996**, *35*, 15383−15390.
(35) Dai, J.; Chen, D.; Jones, R. A.; Hurley, L. H.; Yang, D. NMR solution structure of the major G-quadruplex structure formed in the human BCL2 promoter region. *Nucleic Acids Res.* **2006**, *34*, 5133−5144.
(36) Adrian, M.; Heddi, B.; Phan, A. T. NMR spectroscopy of G-quadruplexes. *Methods* **2012**, *57*, 11−24.
(37) Andrushchenko, V.; Leonenko, Z.; Cramb, D.; van de Sande, H.; Wieser, H. Vibrational CD (VCD) and atomic force microscopy (AFM) study of DNA interaction with Cr3+ ions: VCD and AFM evidence of DNA condensation. *Biopolymers* **2002**, *61*, 243−260.
(38) Andrushchenko, V.; Van De Sande, J. H.; Wieser, H. Vibrational circular dichroism and IR absorption of DNA complexes with Cu2+ ions. *Biopolymers* **2003**, *72*, 374−390.
(39) Polyanichko, A. M.; Andrushchenko, V.; Chikhirzhina, E.; Vorob'ev, V.; Wieser, H. The effect of manganese (II) on DNA structure: electronic and vibrational circular dichroism studies. *Nucleic Acids Res.* **2004**, *32*, 989−996.
(40) Tsankov, D.; Krasteva, M.; Andrushchenko, V.; van de Sande, J.; Wieser, H. Vibrational circular dichroism signature of hemi-protonated intercalated four-stranded i-DNA. *Biophys. Chem.* **2006**, *119*, 1−6.
(41) Nový, J.; Böhm, S.; Králová, J.; Král, V.; Urbanová, M. Formation and temperature stability of G-quadruplex structures studied by electronic and vibrational circular dichroism spectroscopy combined with ab initio calculations. *Biopolymers* **2008**, *89*, 144−152.
(42) Andrushchenko, V.; Tsankov, D.; Krasteva, M.; Wieser, H.; Bour, P. Spectroscopic detection of DNA quadruplexes by vibrational circular dichroism. *J. Am. Chem. Soc.* **2011**, *133*, 15055−15064.
(43) Bell, A. F.; Hecht, L.; Barron, L. Vibrational Raman optical activity of DNA and RNA. *J. Am. Chem. Soc.* **1998**, *120*, 5820−5821.
(44) Blanch, E. W.; Hecht, L.; Barron, L. D. Vibrational Raman optical activity of proteins, nucleic acids, and viruses. *Methods* **2003**, *29*, 196−209.
(45) Barron, L. D. The development of biomolecular Raman optical activity spectroscopy. *Biomed. Spectrosc. Imaging* **2015**, *4*, 223−253.
(46) Gąsior-Głogowska, M.; Malek, K.; Zajac, G.; Baranska, M. A new insight into the interaction of cisplatin with DNA: ROA spectroscopic studies on the therapeutic effect of the drug. *Analyst* **2016**, *141*, 291−296.
(47) Tan, J.; Zhang, J.; Li, C.; Luo, Y.; Ye, S. Ultrafast energy relaxation dynamics of amide I vibrations coupled with protein-bound water molecules. *Nat. Commun.* **2019**, *10*, No. 1010.
(48) Pal, S. K.; Zhao, L.; Zewail, A. H. Water at DNA surfaces: Ultrafast dynamics in minor groove recognition. *Proc. Natl. Acad. Sci. U.S.A.* **2003**, *100*, 8113.
(49) Chou, S. G.; DeCamp, M. F.; Jiang, J.; Samsonidze, G. G.; Barros, E. B.; Plentz, F.; Jorio, A.; Zheng, M.; Onoa, G. B.; Semke, E. D.; Tokmakoff, A.; Saito, R.; Dresselhaus, G.; Dresselhaus, M. S. Phonon-assisted exciton relaxation dynamics for a (6,5)-enriched DNA-wrapped single-walled carbon nanotube sample. *Phys. Rev. B* **2005**, *72*, No. 195415.
(50) Simpson, G. J. Molecular origins of the remarkable chiral sensitivity of second-order nonlinear optics. *ChemPhysChem* **2004**, *5*, 1301−1310.
(51) Chung, C.-Y.; Potma, E. O. Biomolecular Imaging with Coherent Nonlinear Vibrational Microscopy. *Annu. Rev. Phys. Chem.* **2013**, *64*, 77−99.
(52) Di Antonio, M.; Ponjavic, A.; Radzevičius, A.; Ranasinghe, R. T.; Catalano, M.; Zhang, X.; Shen, J.; Needham, L.-M.; Lee, S. F.; Klenerman, D.; Balasubramanian, S. Single-molecule visualization of DNA G-quadruplex formation in live cells. *Nat. Chem.* **2020**, *12*, 832−837.
(53) Sartenaer, Y.; Tourillon, G.; Dreesen, L.; Lis, D.; Mani, A. A.; Thiry, P. A.; Peremans, A. Sum-frequency generation spectroscopy of DNA monolayers. *Biosens. Bioelectron.* **2007**, *22*, 2179−2183.
(54) Howell, C.; Schmidt, R.; Kurz, V.; Koelsch, P. Sum-frequency-generation spectroscopy of DNA films in air and aqueous environments. *Biointerphases* **2008**, *3*, FC47−FC51.
(55) Guyot-Sionnest, P.; Hunt, J. H.; Shen, Y. R. Sum-frequency vibrational spectroscopy of a Langmuir film: Study of molecular orientation of a two-dimensional system. *Phys. Rev. Lett.* **1987**, *59*, 1597−1600.
(56) Goh, M. C.; Hicks, J.; Kemnitz, K.; Pinto, G.; Heinz, T.; Eisenthal, K.; Bhattacharyya, K. Absolute orientation of water molecules at the neat water surface. *J. Phys. Chem. A* **1988**, *92*, 5074−5075.
(57) Shen, Y. R. Surface properties probed by second-harmonic and sum-frequency generation. *Nature* **1989**, *337*, 519−525.
(58) Richmond, G. L. Molecular Bonding and Interactions at Aqueous Surfaces as Probed by Vibrational Sum Frequency Spectroscopy. *Chem. Rev.* **2002**, *102*, 2693−2724.
(59) Walker, D. S.; Richmond, G. L. Interfacial Depth Profiling of the Orientation and Bonding of Water Molecules across Liquid−Liquid Interfaces. *J. Phys. Chem. C* **2008**, *112*, 201−209.
(60) Rao, Y.; Hong, S.-Y.; Turro, N. J.; Eisenthal, K. B. Molecular orientational distribution at interfaces using second harmonic generation. *J. Phys. Chem. C* **2011**, *115*, 11678−11683.
(61) Shen, L.; Ulrich, N. W.; Mello, C. M.; Chen, Z. Determination of conformation and orientation of immobilized peptides and proteins at buried interfaces. *Chem. Phys. Lett.* **2015**, *619*, 247−255.
(62) Simpson, G. J. *Nonlinear Optical Polarization Analysis in Chemistry and Biology*; Cambridge University Press, 2017.
(63) Wei, S.; Zou, X.; Tian, J.; Huang, H.; Guo, W.; Chen, Z. Control of Protein Conformation and Orientation on Graphene. *J. Am. Chem. Soc.* **2019**, *141*, 20335−20343.
(64) Zhang, G.; Surwade, S. P.; Zhou, F.; Liu, H. DNA nanostructure meets nanofabrication. *Chem. Soc. Rev.* **2013**, *42*, 2488−2496.
(65) Payne, A. C.; Andregg, M.; Kemmish, K.; Hamalainen, M.; Bowell, C.; Bleloch, A.; Klejwa, N.; Lehrach, W.; Schatz, K.; Stark, H.; Marblestone, A.; Church, G.; Own, C. S.; Andregg, W. Molecular threading: mechanical extraction, stretching and placement of DNA molecules from a liquid-air interface. *PLoS One* **2013**, *8*, No. e69058.
(66) Bensimon, A.; Simon, A.; Chiffaudel, A.; Croquette, V.; Heslot, F.; Bensimon, D. Alignment and Sensitive Detection of DNA by a Moving Interface. *Science* **1994**, *265*, 2096−2098.
(67) Weler, H. U. G.; Wang, L.; Mullikin, J. C.; Zhu, Y.; Cheng, J. F.; Greulich, K. M.; Bensimon, A.; Gray, J. W. Quantitative DNA fiber mapping. *Hum. Mol. Genet.* **1995**, *4*, 1903−1910.
(68) Michalet, X.; Ekong, R.; Fougerousse, F.; Rousseaux, S.; Schurra, C.; Hornigold, N.; Slegtenhorst Marjon, V.; Wolfe, J.; Povey, S.; Beckmann Jacques, S.; Bensimon, A. Dynamic Molecular Combing: Stretching the Whole Human Genome for High-Resolution Studies. *Science* **1997**, *277*, 1518−1523.
(69) Bell, D. C.; Thomas, W. K.; Murtagh, K. M.; Dionne, C. A.; Graham, A. C.; Anderson, J. E.; Glover, W. R. DNA Base Identification by Electron Microscopy. *Microsc. Microanal.* **2012**, *18*, 1049−1053.

https://doi.org/10.1021/acs.langmuir.2c00365
Langmuir XXXX, XXX, XXX−XXX

(70) Frommer, M. A.; Miller, I. Adsorption of DNA at the air-water interface. *J. Phys. Chem. B* **1968**, *72*, 2862−2866.
(71) Douarche, C.; Sikorav, J. L.; Goldar, A. Aggregation and Adsorption at the Air-Water Interface of Bacteriophage ϕX174 Single-Stranded DNA. *Biophys. J.* **2008**, *94*, 134−146.
(72) Morasch, M.; Liu, J.; Dirscherl, C. F.; Ianeselli, A.; Kühnlein, A.; Le Vay, K.; Schwintek, P.; Islam, S.; Corpinot, M. K.; Scheu, B.; Dingwell, D. B.; Schwille, P.; Mutschler, H.; Powner, M. W.; Mast, C. B.; Braun, D. Heated gas bubbles enrich, crystallize, dry, phosphorylate and encapsulate prebiotic molecules. *Nat. Chem.* **2019**, *11*, 779−788.
(73) Taillandier, E.; Liquier, J. [16] Infrared Spectroscopy of DNA. In *Methods in Enzymology*; Academic Press, 1992; Vol. *211*, pp 307−335.
(74) Nakamoto, K.; Tsuboi, M.; Strahan, G. D. *Drug-DNA Interactions: Structures and Spectra*; John Wiley & Sons, 2008.
(75) Peng, C. S.; Jones, K. C.; Tokmakoff, A. Anharmonic Vibrational Modes of Nucleic Acid Bases Revealed by 2D IR Spectroscopy. *J. Am. Chem. Soc.* **2011**, *133*, 15650−15660.
(76) Yang, M.; Szyc, Ł.; Elsaesser, T. Femtosecond Two-Dimensional Infrared Spectroscopy of Adenine-Thymine Base Pairs in DNA Oligomers. *J. Phys. Chem. B* **2011**, *115*, 1262−1267.
(77) Wood, B. R. The importance of hydration and DNA conformation in interpreting infrared spectra of cells and tissues. *Chem. Soc. Rev.* **2016**, *45*, 1980−1998.
(78) Hithell, G.; González-Jiménez, M.; Greetham, G. M.; Donaldson, P. M.; Towrie, M.; Parker, A. W.; Burley, G. A.; Wynne, K.; Hunt, N. T. Ultrafast 2D-IR and optical Kerr effect spectroscopy reveal the impact of duplex melting on the structural dynamics of DNA. *Phys. Chem. Chem. Phys.* **2017**, *19*, 10333−10342.
(79) Sanstead, P. J.; Tokmakoff, A. Direct Observation of Activated Kinetics and Downhill Dynamics in DNA Dehybridization. *J. Phys. Chem. B* **2018**, *122*, 3088−3100.
(80) Barhoumi, A.; Zhang, D.; Tam, F.; Halas, N. J. Surface-Enhanced Raman Spectroscopy of DNA. *J. Am. Chem. Soc.* **2008**, *130*, 5523−5529.
(81) Xu, L.-J.; Lei, Z.-C.; Li, J.; Zong, C.; Yang, C. J.; Ren, B. Label-Free Surface-Enhanced Raman Spectroscopy Detection of DNA with Single-Base Sensitivity. *J. Am. Chem. Soc.* **2015**, *137*, 5149−5154.
(82) Studdert, D. S.; Davis, R. C. Calculations of the circular dichroism of double-helical nucleic acids. I. Effects involving $\pi \rightarrow \pi^*$ transitions. *Biopolymers* **1974**, *13*, 1377−1389.
(83) Studdert, D. S.; Davis, R. C. Calculations of the circular dichroism of double-helical nucleic acids. II. Effects involving n$\rightarrow \pi^*$ transitions. *Biopolymers* **1974**, *13*, 1391−1403.
(84) Studdert, D. S.; Davis, R. C. Calculation of the circular dichroism of double-helical nucleic acids. III. Dependence of the results on the choice of wave functions for purines and pyrimidines. *Biopolymers* **1974**, *13*, 1405−1416.
(85) Johnson, B. B.; Dahl, K. S.; Tinoco, I., Jr; Ivanov, V. I.; Zhurkin, V. B. Correlations between deoxyribonucleic acid structural parameters and calculated circular dichroism spectra. *Biochemistry* **1981**, *20*, 73−78.
(86) Steely, H. T., Jr.; Gray, D. M.; Ratliff, R. L. CD of homopolymer DNA-RNA hybrid duplexes and triplexes containing A.T or A.U base pairs. *Nucleic Acids Res.* **1986**, *14*, 10071−10090.
(87) Alexeev, D. G.; Lipanov, A. A.; Skuratovskii, I. Y. Poly(dA)-mpoly(dT) is a B-type double helix with a distinctively narrow minor groove. *Nature* **1987**, *325*, 821−823.
(88) Stokes, G. Y.; Gibbs-Davis, J. M.; Boman, F. C.; Stepp, B. R.; Condie, A. G.; Nguyen, S. T.; Geiger, F. M. Making "Sense" of DNA. *J. Am. Chem. Soc.* **2007**, *129*, 7492−7493.
(89) Walter, S. R.; Geiger, F. M. DNA on Stage: Showcasing Oligonucleotides at Surfaces and Interfaces with Second Harmonic and Vibrational Sum Frequency Generation. *J. Phys. Chem. Lett.* **2010**, *1*, 9−15.
(90) Li, Z.; Weeraman, C. N.; Azam, M. S.; Osman, E.; Gibbs-Davis, J. M. The thermal reorganization of DNA immobilized at the silica/buffer interface: a vibrational sum frequency generation investigation. *Phys. Chem. Chem. Phys.* **2015**, *17*, 12452−12457.
(91) Pilet, J.; Blicharski, J.; Brahms, J. Conformations and structural transitions in polydeoxynucleotides. *Biochemistry* **1975**, *14*, 1869−1876.
(92) Marky, L. A.; Kupke, D. W. Probing the hydration of the minor groove of A:T synthetic DNA polymers by volume and heat changes. *Biochemistry* **1989**, *28*, 9982−9988.
(93) Iyer, V.; Struhl, K. Poly(dA:dT), a ubiquitous promoter element that stimulates transcription via its intrinsic DNA structure. *EMBO J.* **1995**, *14*, 2570−2579.
(94) Rich, A.; Davies, D. R.; Crick, F. H. C.; Watson, J. D. The molecular structure of polyadenylic acid. *J. Mol. Biol.* **1961**, *3*, 71−86.
(95) Safaee, N.; Noronha, A. M.; Rodionov, D.; Kozlov, G.; Wilds, C. J.; Sheldrick, G. M.; Gehring, K. Structure of the Parallel Duplex of Poly(A) RNA: Evaluation of a 50 Year-Old Prediction. *Angew. Chem., Int. Ed.* **2013**, *52*, 10370−10373.
(96) Westhof, E.; Sundaralingam, M. X-ray-structure of a cytidylyl-3′,5′-adenosine-proflavine complex: a self-paired parallel-chain double helical dimer with an intercalated acridine dye. *Proc. Natl. Acad. Sci. U.S.A.* **1980**, *77*, 1852.
(97) Luo, J.; Sarma, M. H.; Yuan, R.-d.; Sarma, R. H. NMR study of self-paired parallel duplex of d(AAAAACCCCC) in solution. *FEBS Lett.* **1992**, *306*, 223−228.
(98) Rippe, K.; Fritsch, V.; Westhof, E.; Jovin, T. M. Alternating d(G-A) sequences form a parallel-stranded DNA homoduplex. *EMBO J.* **1992**, *11*, 3777−3786.
(99) Robinson, H.; Van der Marel, G. A.; Van Boom, J. H.; Wang, A. H. J. Unusual DNA conformation at low pH revealed by NMR: parallel-stranded DNA duplex with homo base pairs. *Biochemistry* **1992**, *31*, 10510−10517.
(100) Robinson, H.; Wang, A. H. 5′-CGA sequence is a strong motif for homo base-paired parallel-stranded DNA duplex as revealed by NMR analysis. *Proc. Natl. Acad. Sci. U.S.A.* **1993**, *90*, 5224.
(101) Germann, M. W.; Zhou, N.; van de Sande, J. H.; Vogel, H. J. [9] Parallel-Stranded Duplex DNA: An NMR Perspective. In *Methods in Enzymology*; Academic Press, 1995; Vol. *261*, pp 207−225.
(102) Chakraborty, S.; Sharma, S.; Maiti, P. K.; Krishnan, Y. The poly dA helix: a new structural motif for high performance DNA-based molecular switches. *Nucleic Acids Res.* **2009**, *37*, 2810−2817.
(103) Huang, Z.; Liu, B.; Liu, J. Parallel Polyadenine Duplex Formation at Low pH Facilitates DNA Conjugation onto Gold Nanoparticles. *Langmuir* **2016**, *32*, 11986−11992.
(104) Ma, G.; Liu, J.; Fu, L.; Yan, E. C. Y. Probing Water and Biomolecules at the Air—Water Interface with a Broad Bandwidth Vibrational Sum Frequency Generation Spectrometer from 3800 to 900 cm−1. *Appl. Spectrosc.* **2009**, *63*, 528−537.
(105) Chen, S.-L.; Fu, L.; Gan, W.; Wang, H.-F. Homogeneous and inhomogeneous broadenings and the Voigt line shapes in the phase-resolved and intensity sum-frequency generation vibrational spectroscopy. *J. Chem. Phys.* **2016**, *144*, No. 034704.
(106) Black, J. W.; Kamenetska, M.; Ganim, Z. An Optical Tweezers Platform for Single Molecule Force Spectroscopy in Organic Solvents. *Nano Lett.* **2017**, *17*, 6598−6605.
(107) Barth, A.; Zscherp, C. What vibrations tell about proteins. *Q. Rev. Biophys.* **2002**, *35*, 369−430.
(108) Tsuboi, M. Application of Infrared Spectroscopy to Structure Studies of Nucleic Acids. *Appl. Spectrosc. Rev.* **1970**, *3*, 45−90.
(109) Lacher, J. R.; Bitner, J. L.; Emery, D. J.; Seffl, M. E.; Park, J. D. The Infrared Absorption Spectra of Some Substituted Purines and Pyrimidines in Antimony Trichloride Solution. *J. Phys. Chem. C* **1955**, *59*, 615−625.
(110) Kyogoku, Y.; Lord, R. C.; Rich, A. An Infrared Study of Hydrogen Bonding between Adenine and Uracil Derivatives in Chloroform Solution. *J. Am. Chem. Soc.* **1967**, *89*, 496−504.
(111) Stepanian, S. G.; Sheina, G. G.; Radchenko, E. D.; Blagoi, Y. P. Theoretical and experimental studies of adenine, purine and pyrimidine isolated molecule structure. *J. Mol. Struct.* **1985**, *131*, 333−346.

https://doi.org/10.1021/acs.langmuir.2c00365
Langmuir XXXX, XXX, XXX−XXX

(112) Florián, J. Scaled quantum mechanical force fields and interpretation of vibrational spectra of differently protonated adenine. *J. Mol. Struct.: THEOCHEM* **1992**, *253*, 83−100.
(113) Dhaouadi, Z.; Ghomi, M.; Austin, J. C.; Girling, R. B.; Hester, R. E.; Mojzes, P.; Chinsky, L.; Turpin, P. Y.; Coulombeau, C.; Jobic, H.; Tomkinson, J. Vibrational motions of bases of nucleic acids as revealed by neutron inelastic scattering and resonance Raman spectroscopy. 1. Adenine and its deuterated species. *J. Phys. Chem. D* **1993**, *97*, 1074−1084.
(114) Dovbeshko, G.; Fesenko, O.; Dementjev, A.; Karpicz, R.; Fedorov, V.; Posudievsky, O. Y. Coherent anti-Stokes Raman scattering enhancement of thymine adsorbed on graphene oxide. *Nanoscale Res. Lett.* **2014**, *9*, No. 263.
(115) Superfine, R.; Huang, J. Y.; Shen, Y. R. Phase measurement for surface infrared−visible sum-frequency generation. *Opt. Lett.* **1990**, *15*, 1276−1278.
(116) Yamaguchi, S.; Otosu, T. Progress in phase-sensitive sum frequency generation spectroscopy. *Phys. Chem. Chem. Phys.* **2021**, *23*, 18253−18267.
(117) Hopkins, H. P.; Hamilton, D. D.; Wilson, W. D.; Zon, G. Duplex and triple helix formation with dA19 and dT19: thermodynamic parameters from calorimetric, NMR, and circular dichroism studies. *J. Phys. Chem. E* **1993**, *97*, 6555−6563.
(118) Ye, S.; Noda, H.; Nishida, T.; Morita, S.; Osawa, M. Cd2+-Induced Interfacial Structural Changes of Langmuir−Blodgett Films of Stearic Acid on Solid Substrates: A Sum Frequency Generation Study. *Langmuir* **2004**, *20*, 357−365.
(119) Nakano, S.-i.; Miyoshi, D.; Sugimoto, N. Effects of Molecular Crowding on the Structures, Interactions, and Functions of Nucleic Acids. *Chem. Rev.* **2014**, *114*, 2733−2758.
(120) Asanuma, H.; Noguchi, H.; Uosaki, K.; Yu, H.-Z. Metal Cation-Induced Deformation of DNA Self-Assembled Monolayers on Silicon: Vibrational Sum Frequency Generation Spectroscopy. *J. Am. Chem. Soc.* **2008**, *130*, 8016−8022.
(121) Ho, J.-J.; Skoff, D. R.; Ghosh, A.; Zanni, M. T. Structural Characterization of Single-Stranded DNA Monolayers Using Two-Dimensional Sum Frequency Generation Spectroscopy. *J. Phys. Chem. B* **2015**, *119*, 10586−10596.
(122) McDermott, M. L.; Vanselous, H.; Corcelli, S. A.; Petersen, P. B. DNA's Chiral Spine of Hydration. *ACS Cent. Sci.* **2017**, *3*, 708−714.
(123) Taton, T. A.; Mirkin Chad, A.; Letsinger Robert, L. Scanometric DNA Array Detection with Nanoparticle Probes. *Science* **2000**, *289*, 1757−1760.
(124) Huertas, C. S.; Calvo-Lozano, O.; Mitchell, A.; Lechuga, L. M. Advanced Evanescent-Wave Optical Biosensors for the Detection of Nucleic Acids: An Analytic Perspective. *Front. Chem.* **2019**, *7*, No. 724.
(125) Liu, W.; Fu, L.; Wang, Z.; Sohrabpour, Z.; Li, X.; Liu, Y.; Wang, H.-f.; Yan, E. C. Y. Two dimensional crowding effects on protein folding at interfaces observed by chiral vibrational sum frequency generation spectroscopy. *Phys. Chem. Chem. Phys.* **2018**, *20*, 22421−22426.
(126) Wurpel, G. W. H.; Sovago, M.; Bonn, M. Sensitive Probing of DNA Binding to a Cationic Lipid Monolayer. *J. Am. Chem. Soc.* **2007**, *129*, 8420−8421.
(127) Singh, P. C.; Ahmed, M.; Nihonyanagi, S.; Yamaguchi, S.; Tahara, T. DNA-Induced Reorganization of Water at Model Membrane Interfaces Investigated by Heterodyne-Detected Vibrational Sum Frequency Generation Spectroscopy. *J. Phys. Chem. B* **2022**, *126*, 840−846.
(128) Hu, X.-H.; Fu, L.; Hou, J.; Zhang, Y.-N.; Zhang, Z.; Wang, H.-F. N−H Chirality in Folded Peptide LK7β Is Governed by the Cα−H Chirality. *J. Phys. Chem. Lett.* **2020**, *11*, 1282−1290.
(129) Ohto, T.; Usui, K.; Hasegawa, T.; Bonn, M.; Nagata, Y. Toward ab initio molecular dynamics modeling for sum-frequency generation spectra; an efficient algorithm based on surface-specific velocity-velocity correlation function. *J. Chem. Phys.* **2015**, *143*, No. 124702.
(130) Morita, A.; Hynes, J. T. A Theoretical Analysis of the Sum Frequency Generation Spectrum of the Water Surface. II. Time-Dependent Approach. *J. Phys. Chem. B* **2002**, *106*, 673−685.
(131) Auer, B. M.; Skinner, J. L. Dynamical effects in line shapes for coupled chromophores: Time-averaging approximation. *J. Chem. Phys.* **2007**, *127*, No. 104105.
(132) Auer, B. M.; Skinner, J. L. IR and Raman spectra of liquid water: Theory and interpretation. *J. Chem. Phys.* **2008**, *128*, No. 224511.
(133) Auer, B. M.; Skinner, J. L. Vibrational Sum-Frequency Spectroscopy of the Water Liquid/Vapor Interface. *J. Phys. Chem. B* **2009**, *113*, 4125−4130.
(134) Pieniazek, P. A.; Tainter, C. J.; Skinner, J. L. Interpretation of the water surface vibrational sum-frequency spectrum. *J. Chem. Phys.* **2011**, *135*, No. 044701.

https://doi.org/10.1021/acs.langmuir.2c00365
Langmuir XXXX, XXX, XXX−XXX